Chinese Journal of
POLYMER SCIENCE

RESEARCH ARTICLE

https://doi.org/10.1007/s10118-026-3779-2
Chinese J. Polym. Sci.

Chemically Bonding Metal Atoms into a Polymer Chain

Zihao Zhao†, Fuyao Huang†, Yifeng Zhang, and Huisheng Peng*

State Key Laboratory of Molecular Engineering of Polymers, Department of Macromolecular Science, and Institute of Fiber Materials and Devices, Fudan University, Shanghai 200438, China

Electronic Supplementary Information

Abstract Metal-backboned polymers have been proposed as a new class of materials with remarkable physical and chemical properties for applications in optoelectronics, magnetism, and energy. However, the number of metal atoms in their backbones is limited to less than 30 to date. This has prevented the systematic investigation of their properties. Herein, we report the synthesis of metal-backboned polymers with a polymerization degree of 169. Using gold as a model system, we identified that the controlled release of Ag^+, an electron-donating imidazole co-ligand, ligand steric/electronic effects, and elevated reaction temperature are key to achieving such long chains. The resulting metal-backboned polymers display hallmark polymer behaviors such as glass transition, together with a unique electronic structure featuring pronounced electron delocalization along the Au backbone and efficient room-temperature phosphorescence. This work provides an effective route to long-chain metal-backboned polymers and deepens the understanding of the electronic structures in one-dimensional metal backbones.

Keywords Metal backbone; Gold–gold bond; Electron delocalization; Gold-backboned polymer; Degree of polymerization

Citation: Zhao, Z.; Huang, F.; Zhang, Y.; Peng, H. Chemically bonding metal atoms into a polymer chain. *Chinese J. Polym. Sci.* https://doi.org/10.1007/s10118-026-3779-2

INTRODUCTION

Metal-backboned polymers, featuring one-dimensional single-atom metal chains with backbones composed of metal atoms linked by consecutive metal–metal bonds, have been proposed as a new class of polymeric materials.[1–3] This unique architecture endows them with appealing optoelectronic properties, opening avenues for applications in flexible electronics, microwave absorption, and photocatalysis.[4–7] Nonetheless, the synthesis of long-chain metal-backboned polymers has long been hampered by the intrinsic weakness of metal-metal bonds and the tendency of metal atoms to adopt close-packed structures.[8–10] Early efforts employing cage-like multidentate bridging ligands achieved controlled chain elongation to some extent, but suffered from tedious ligand synthesis and increased probability of metal miscoordination with chain extension, leading to low degrees of polymerization (DP).[1–3] Recently, we developed a one-pot synthesis strategy for metal atoms that possess sufficiently strong interactions,[11] demonstrating the viability of this straightforward method. However, control over DP and the optimization of even longer chains remain largely unexplored in this system.

Herein, we systematically investigated the influence of reagents and conditions on the formation and stabilization of the metal backbone using gold atoms as a demonstration (Scheme 1). Through a series of controlled experiments, we identified several favorable factors for achieving high DPs: slow release of Ag^+, electron-donating imidazole, low steric hindrance of the bisphosphine ligand, and elevated reaction temperature. After optimization, we successfully synthesized metal-backboned polymers with a record-high DP of 169. The resulting gold-backboned polymer (GBP) exhibited efficient electron delocalization along the one-dimensional Au backbone and typical polymer characteristics such as glass transition. These findings reveal the key factors governing the polymerization of GBPs and provide a new strategy for constructing long-chain metal-backboned polymers.

EXPERIMENTAL

The details of experiments are included in the electronic supplementary information (ESI).

RESULTS AND DISCUSSION

Before polymerization, a dinuclear gold precursor was synthesized using a bisphosphine ligand (DPPM or DCPM) and (dimethyl sulfide) gold(I) chloride (Fig. S1 in ESI).[12,13] Polymerization was initiated by chloride abstraction upon the addition of Ag^+, generating highly reactive dicationic species that can be stabilized by the coordination of two imidazole derivatives (N-MeIm or N-AcIm). Subsequently, one gold center was eliminated as a stable bis-imidazole complex (intermediate **A**), yielding a

* Corresponding author, E-mail: penghs@fudan.edu.cn
† These authors contributed equally to this work.
Received May 22, 2026; Accepted June 10, 2026; Published online August 3, 2026

four-membered chelate (intermediate **B**). Driven by strong and long-range Au—Au interactions, intermediate **B** undergoes chain propagation *via* ordered Au—Au bonds, thus forming GBP (Scheme 1).[11] To systematically investigate the factors influencing this polymerization and optimize the chain length, several key reaction parameters, such as the bisphosphine ligand, imidazole derivative, silver salt ($AgNO_3$, $AgBF_4$, and $AgPF_6$), and reaction temperature, were adopted for comparative experiments.

First, the influence of the silver salt and imidazole derivatives on the polymerization outcome was evaluated (Table 1 and Fig. S2 in ESI). When $AgNO_3$ was used as the silver source, the resulting GBP exhibited a weight-average molecular weight (M_w) of 33.5 kDa. In contrast, replacing $AgNO_3$ with $AgBF_4$ or $AgPF_6$ led to drastically lower M_ws of 12.6 and 11.9 kDa, respectively. This was ascribed to the higher solubility of $AgBF_4$ and $AgPF_6$ in the reaction solvent (dichloromethane). The rapid release of Ag^+ generated an extremely high local concentration of intermediate **B**, which tended to disrupt the balance between chain propagation and termination, thus limiting the molecular weight. Conversely, the lower solubility of $AgNO_3$ maintained a stable heterogeneous reaction interface with a slower but sustained release of Ag^+, ensuring a smooth and controlled polymerization process (Fig. S3 and Note S1 in ESI).

The electronic nature of the imidazole derivatives also plays a crucial role. Under otherwise identical conditions ($AgNO_3$ as the silver source), replacing the imidazole derivative N-MeIm with N-AcIm led to a marked decrease in molecular weight from 33.5 kDa to 22.3 kDa (Table 1). This can be rationalized by considering the key intermediate **A**. Because of the electron-deficient nature of the Au^+ center, N-AcIm with an electron-withdrawing acetyl group was unfavorable for the stability of intermediate **A**. This shifted the equilibrium away from the formation of intermediate **B**, thereby hindering chain growth. Remarkably, in the absence of imidazole, only low-molecular-weight species were detected (M_w<3 kDa, Fig. S4 in ESI), indicating that no efficient chain propagation occurred, highlighting the essential role of imidazole derivatives in polymerization. These results indicate that an imidazole derivative with moderate electron-donating ability is beneficial for efficient polymerization of GBP.

After establishing $AgNO_3$ and N-MeIm as the optimized reagents, the influence of the bisphosphine ligand and reaction temperature on the polymerization outcome was further examined (Table 2, Figs. 1a, 1b, and Table S1 in ESI). Compared with the polymer with aromatic ligand DPPM (**GBP1**), the counterpart (**GBP2**) with alicyclic ligand DCPM demon-

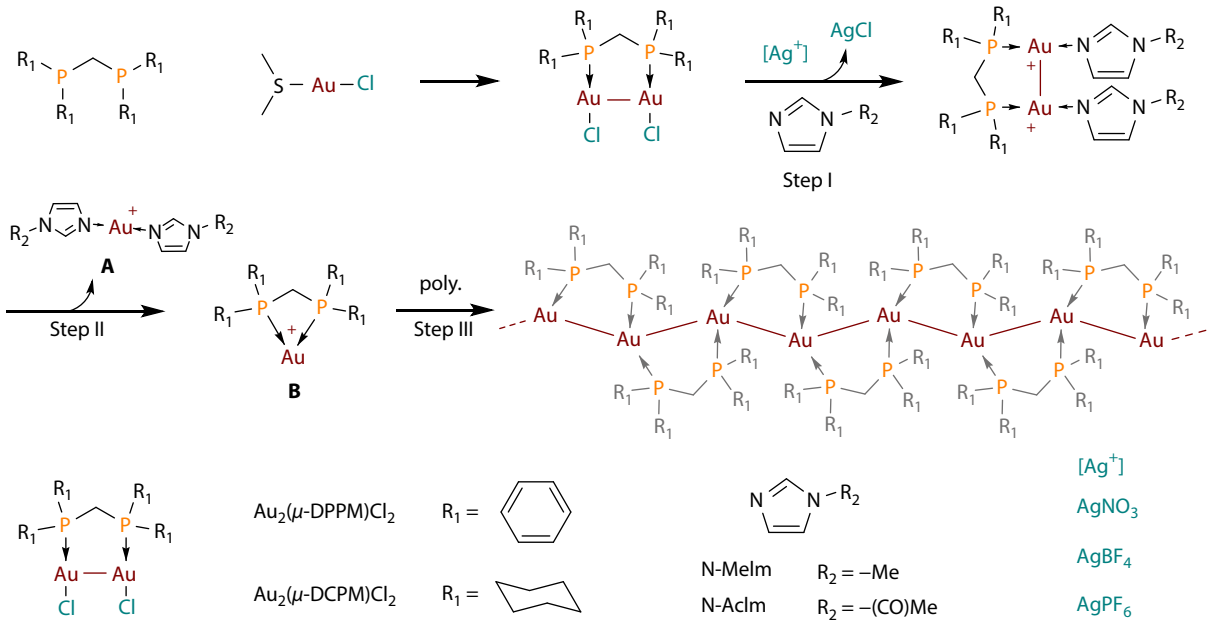

Scheme 1 Structure and synthetic approach to GBP. Step I: chloride abstraction by Ag^+ from the dinuclear precursor. Step II: formation of the bis-imidazole complex (intermediate **A**) and its departure, generating the active four-membered chelate (intermediate **B**). Step III: chain propagation *via* Au—Au bond formation.

Table 1 Effect of imidazole derivative and silver salt on the polymerization of GBP.[a]

Entry	Bisphosphine ligand	Imidazole derivative	Silver salt	M_w[b] (kDa)	DP_w	$Đ$
1	DPPM	N-MeIm	$AgNO_3$	33.5±3.0	58	1.73
2	DPPM	N-MeIm	$AgBF_4$	12.6±0.9	22	2.68
3	DPPM	N-MeIm	$AgPF_6$	11.9±0.5	20	2.71
4	DPPM	N-AcIm	$AgNO_3$	22.3±3.3	38	1.70

[a] Reaction conditions: precursor/imidazole derivative/silver salt = 1/2.2/10, [precursor] = 10 mg/mL, carried out in dichloromethane, T = 25 °C; [b] Determined by gel permeation chromatography coupled with multi-angle laser light scattering using a measured dn/dc value of 0.1418 mL/g.[11]

strated an increased M_w of 65.0 kDa, with a measured d*n*/d*c* value of 0.1108 mL/g (Fig. S5 in ESI), which corresponds to a DP_w of 108. Increasing the reaction temperature can further increase the molecular weight, reaching 53.4 and 104.5 kDa for polymers with ligands DPPM (**GBP3**) and DCPM (**GBP4**), respectively. Remarkably, the DP_w of **GBP4** was calculated to be 169, which represents a new record for metal-backboned polymers.

To monitor the polymerization process, Raman spectra of the dinuclear precursors and the corresponding polymers were recorded (Figs. 1c and 1d). For both $Au_2(\mu$-DPPM$)Cl_2$ and $Au_2(\mu$-DCPM$)Cl_2$, the spectra exhibited strong peaks attributable to Au—Cl stretching vibrations (319 and 325 cm^{-1} for the former; 318 and 331 cm^{-1} for the latter).[14,15] These characteristic peaks were substantially diminished after polymerization, indicating that the vast majority of chloride was removed during the reaction. EDS analysis confirmed the presence of Au, C, and P, and a weak and evenly distributed Cl signal was also detected (Fig. S6 in ESI), which we attributed to the chain-end capping of GBP. Meanwhile, the Au—P-related vibration peaks at 177 and 187 cm^{-1} for $Au_2(\mu$-DPPM$)Cl_2$ and $Au_2(\mu$-DCPM$)Cl_2$, respectively, shifted and split upon polymerization.[16] This phenomenon reflects a fundamental change in the coordination environment of gold: the formation of Au—Au bonds alters the electron density and force field around Au centers, which further modifies the vibrational characteristics of the Au—P bonds. Therefore, the Raman spectra supported the formation of the Au backbone during polymerization.

A comparison of the single crystal structures of the two precursors, $Au_2(\mu$-DPPM$)Cl_2$ and $Au_2(\mu$-DCPM$)Cl_2$,[17,18] provides insight into how the bisphosphine ligand architecture affects the polymerization outcome (Fig. 1e). In $Au_2(\mu$-DCPM$)Cl_2$, the two gold atoms are significantly closer (3.164 Å) than those in $Au_2(\mu$-DPPM$)Cl_2$ (3.341 Å), indicating a stronger interaction between the two Au centers. This preorganized geometry favors subsequent chain propagation through continuous Au—Au bonds. Moreover, unlike the rigid phenyl rings that exert an electron-withdrawing conjugation effect on the P atoms, the flexible cyclohexyl groups possess an electron-donating inductive effect. As a result, DCPM exhibits higher conformational adaptability, which reduces the steric hindrance between ligands during chain growth. Simultaneously, DCPM can effectively increase the electron density on the P atoms, stabilizing the Au—Au bonds and thus promoting the elongation of the Au back-

Table 2 Effect of bisphosphine ligand and reaction temperature on the polymerization of GBP. [a]

Entry	Sample	Bisphosphine ligand	*T* (°C)	M_w [b] (kDa)	DP_w [c]	*Đ*
1	**GBP1**	DPPM	25	33.5±3.0	58	1.73
5	**GBP2**	DCPM	25	65.0±9.6	108	1.96
6	**GBP3**	DPPM	65	53.4±3.3	92	2.55
7	**GBP4**	DCPM	65	104.5±6.5	169	2.14

[a] Reaction conditions: precursor/imidazole derivative/silver salt = 1/2.2/10, [precursor] = 10 mg/mL, carried out in dichloromethane (*T*=25 °C) or chloroform (*T* = 65 °C); [b] Determined by gel permeation chromatography coupled with multi-angle laser light scattering using a measured *dn/dc* value of 0.1418 mL/g (for ligand DPPM)[11] or 0.1108 mL/g (for ligand DCPM). [c] Calculated using M_w values.

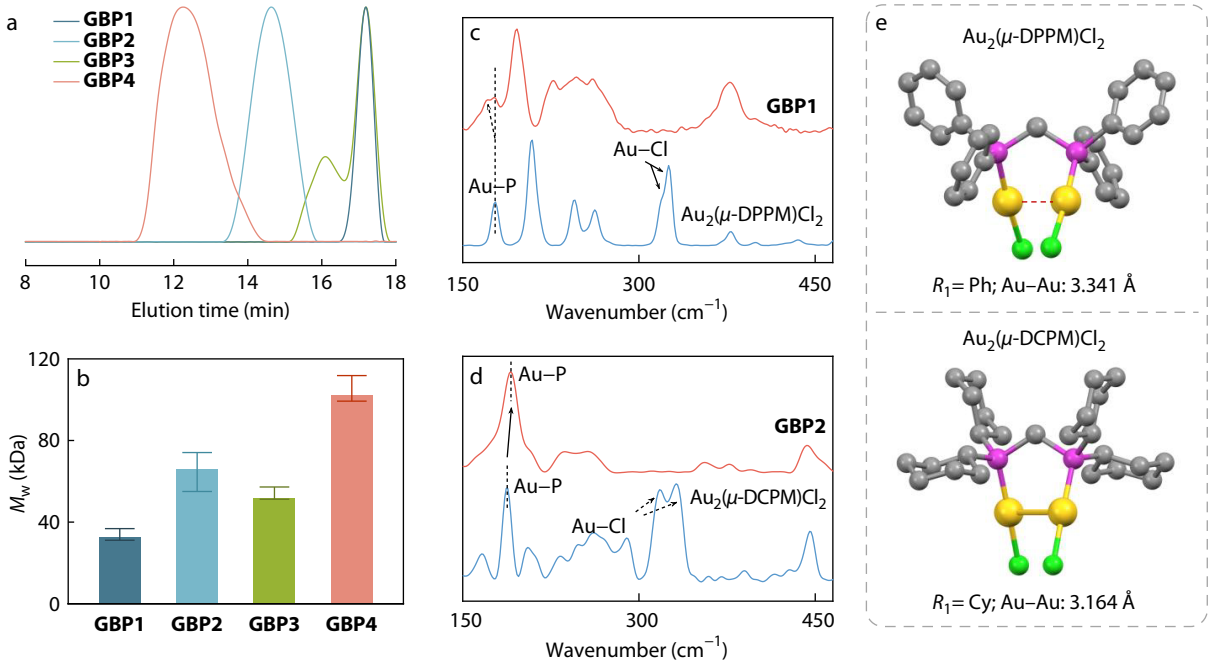

Fig. 1 (a) Gel permeation chromatography coupled with multi-angle laser light scattering curves of **GBP1**–**GBP4** in Table 2; (b) Comparison of M_w of **GBP1**–**GBP4**; (c, d) Raman spectra of GBPs and corresponding precursors (c: $Au_2(\mu$-DPPM$)Cl_2$ and **GBP1**, d: $Au_2(\mu$-DCPM$)Cl_2$ and **GBP2**); (e) Single crystal structure of $Au_2(\mu$-DPPM$)Cl_2$ and $Au_2(\mu$-DCPM$)Cl_2$ and the denoted bond lengths of Au—Au interactions.

https://doi.org/10.1007/s10118-026-3779-2

bone. Similarly, increasing the reaction temperature can also help overcome steric repulsion between the ligands, providing the necessary spatial freedom for Au centers to approach and form bonds. However, it also introduces a higher degree of disorder during polymerization, leading to a broader molecular weight distribution (Fig. 1a).

To verify the targeted one-dimensional Au backbone structure, **GBP2** was selected as a representative sample for further characterization. In contrast to the sharp, well-defined diffraction peaks observed for the crystalline precursor Au_2(μ-DCPM)Cl_2, the X-ray diffraction pattern of **GBP2** exhibited only a broad, diffuse amorphous halo, indicating the loss of long-range order upon polymerization (Fig. 2a). Transmission electron microscopy of **GBP2** revealed a set of strip-like features with a uniform long-axis orientation (Fig. 2b), suggesting a quasi-parallel arrangement of the polymer chains, consistent with the one-dimensional structural motif of GBP. Furthermore, lattice fringes with a spacing of 2.72 Å were observed perpendicular to the stripe direction. This distance fell within the typical range for Au—Au bonds and could thus be assigned to the continuous Au—Au bonds along the Au backbone.[19,20] Notably, no diffraction peaks corresponding to crystalline Au were observed in the X-ray diffraction pattern of **GBP2**. This observation, together with the absence of discrete nanoparticles in transmission electron microscope images, conclusively ruled out the formation of significant amounts of gold clusters or nanoparticles.

Moreover, to capture the chain growth process, we performed matrix-assisted laser desorption/ionization time-of-flight mass spectrometry on the reaction mixture under dilute conditions and short reaction times. A series of oligomeric intermediates, including $Au_4(DCPM)_4$, $Au_5(DCPM)_4$, $Au_5(DCPM)_5$, and $Au_6(DCPM)_5$, was successfully detected (Figs. 2c–2e and Fig. S7 in ESI). The presence of these species

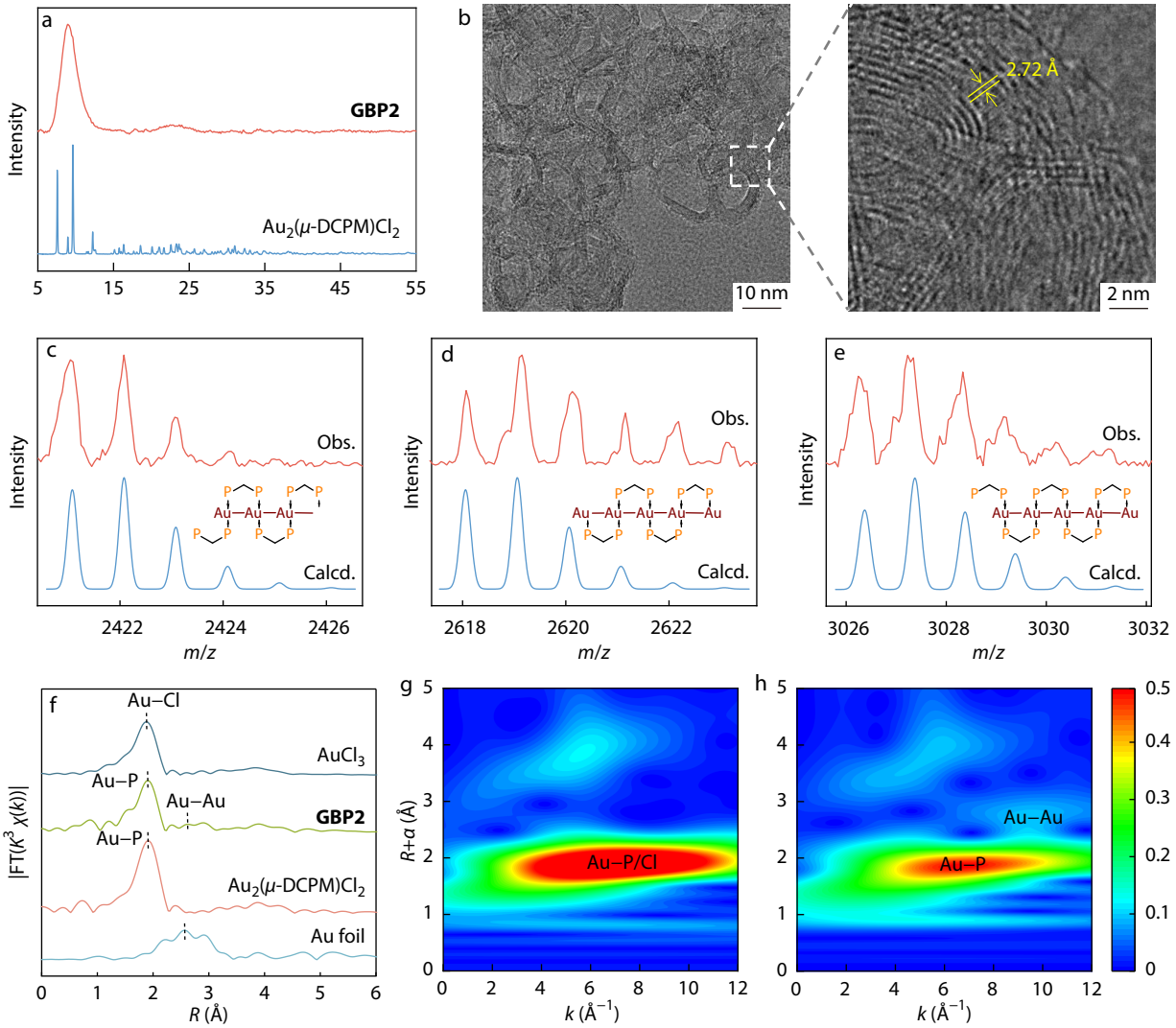

Fig. 2 (a) X-ray diffraction patterns of Au_2(μ-DCPM)Cl_2 and **GBP2**; (b) Transmission electron microscopy images of **GBP2**. Right images: zoomed portions; (c–e) Magnified matrix-assisted laser desorption/ionization time-of-flight mass spectra (observed, obs.) and simulated isotope patterns (calculated, calcd.) of oligomeric intermediates $Au_4(DCPM)_4$, $Au_5(DCPM)_4$, and $Au_5(DCPM)_5$, respectively; (f) Au L_3-edge Fourier-transformed extended X-ray absorption fine structure spectra of Au_2(μ-DCPM)Cl_2 and **GBP2**; (g, h) Wavelet transform contour of extended X-ray absorption fine structure signal for (g) Au_2(μ-DCPM)Cl_2 and (h) **GBP2**.

https://doi.org/10.1007/s10118-026-3779-2

indicates that chain propagation proceeds *via* stepwise addition of $[Au(DCPM)]^+$ units (*i.e.* intermediate **B**), providing direct evidence for the one-dimensional Au backbone and polymerization mechanism.

To obtain direct structural evidence for the Au backbone, we performed Au L_3-edge extended X-ray absorption fine structure measurements on both the precursor $Au_2(\mu$-DCPM)Cl_2 and polymer **GBP2**, together with wavelet transform analysis. Fourier-transformed extended X-ray absorption fine structure spectra show a single prominent peak for the precursor (Fig. 2f, Fig. S8 in ESI), corresponding to the Au—P coordination shell at 2.31 Å with a coordination number of 2.1 (Table S2 in ESI). In contrast, in addition to the Au—P signal, the spectrum of **GBP2** exhibits an additional peak assigned to the Au—Au coordination shell with a bond length of 2.76 Å and a coordination number of 2.0, which is characteristic of one-dimensional Au—Au bonding. Wavelet transform analysis further resolves these contributions. The precursor exhibits a single maximum (Fig. 2g), which is consistent with backscattering from light atoms (P/Cl). Meanwhile, two well-separated intensity maxima for the Au—P and Au—Au bonds were observed in **GBP2** (Fig. 2h), further validating the coexistence of the two distinct coordination environments in **GBP2** and ruling out the possibility that the Au—Au shell arises from Au cluster impurities. The observed coordination environment for each Au center is consistent with the expected one-dimensional structure, which supports the formation of a continuous Au—Au backbone.

The intrinsic thermal properties of **GBP2** were further investigated. Thermogravimetric analysis revealed an onset decomposition temperature (T_d) of about 150 °C, with three distinct weight-loss steps corresponding to low-molecular-weight species evaporation, partial ligand fragmentation, and complete ligand decomposition, respectively (Fig. 3a). Differential scanning calorimetry showed a clear glass transition temperature (T_g) of 47.4 °C (Fig. 3b). This relatively low T_g, attributable to the flexible cyclohexyl rings of the DCPM ligand, indicates segmental mobility of the polymer chains slightly above room temperature. This mobility is consistent with the one-dimensional chain architecture and may facilitate the quasi-parallel chain alignment observed by TEM (Fig. 2b). GBPs bearing the aromatic DPPM ligand (**GBP1** and **GBP3**) show higher T_d (196 and 204 °C, respectively) and T_g (57.6 and 63.6 °C, respectively) compared to their alicyclic DCPM counterparts (**GBP2** and **GBP4**: T_d=150 and 155 °C, T_g=47.4 and 51.3 °C, respectively), reflecting the higher rigidity and thermal stability of the phenyl rings (Figs. S9 and S10 in the ESI).

To investigate the evolution of the electronic structure upon polymerization, the UV-Vis absorption spectra of the diphosphine ligand DCPM, $Au_2(\mu$-DCPM)Cl_2, and **GBP2** were measured. The free DCPM ligand exhibited a sharp absorption peak at 227 nm (Fig. 3c). For the dinuclear complex, in addition to the slightly red-shifted ligand band at 229 nm, a new intense absorption appeared at 246 nm, which was attributed to the $d\sigma^*\rightarrow p\sigma$ metal–metal charge transfer transition arising from the Au—Au interaction between two Au centers.[21] Upon polymerization, this band red-shifted to 252 nm and broadened significantly, indicating enhanced Au—Au interactions and electronic delocalization along the one-dimensional Au backbone. Notably, **GBP2** exhibited a broad absorption envelope in the visible region (400–800 nm), which was absent for both DCPM and $Au_2(\mu$-DCPM)Cl_2 (Fig. 3d). Similar broad absorptions in the visible region were observed for **GBP1**, **GBP3**, and **GBP4** (Fig. S11 in ESI), confirming that the pronounced electronic delocalization along the Au backbone is a general characteristic of

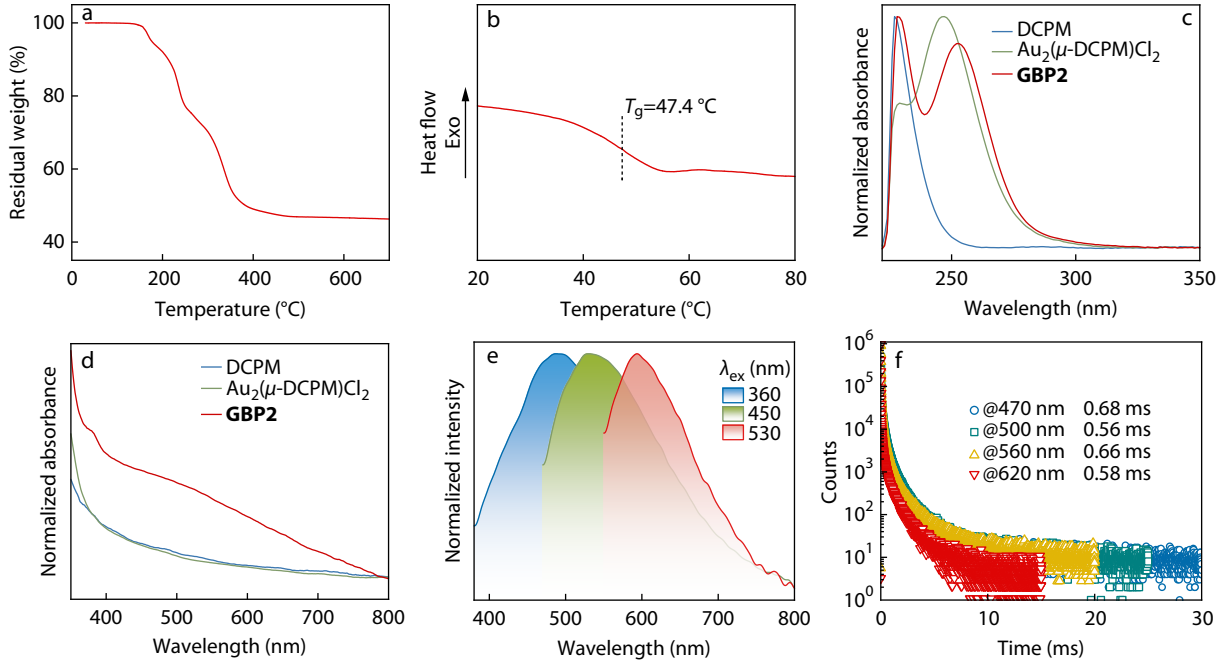

Fig. 3 (a, b) Thermogravimetric analysis and differential scanning calorimetry curves of **GBP2**, respectively; (c, d) Absorption spectra of DCPM, $Au_2(\mu$-DCPM)Cl_2, and **GBP2**. The details in the visible region are stressed in (d); (e, f) Prompt emission spectra and millisecond-scale lifetimes of **GBP2** solid powder (λ_{ex}=360 nm), respectively.

https://doi.org/10.1007/s10118-026-3779-2

these GBPs. Such visible absorption has already emerged for oligomeric trinuclear Au species (Fig. S12 and Note S2 in ESI), and it gradually broadened and extended across the entire 400–800 nm range as the chain length increased to the polymer level. This broad visible absorption is characteristic of the formation of a quasi-band structure,[22] where the bandgap is significantly reduced compared to the HOMO-LUMO gap of the precursor. The spectral evolution from the dinuclear precursor to the polymer provides strong evidence for the formation of a one-dimensional Au backbone, in good agreement with other characterization results.

X-ray photoelectron spectroscopy further supported the electronic structure of the Au backbone. The dinuclear precursor $Au_2(\mu$-DCPM)Cl_2 displays Au $4f_{7/2}$ and $4f_{5/2}$ signals at 85.23 and 88.90 eV (Fig. S13a in ESI), which are characteristic of the formal Au(I) state in a phosphine-coordinated environment. In contrast, **GBP2** shows a symmetric doublet with binding energies of 84.77 eV ($4f_{7/2}$) and 88.47 eV ($4f_{5/2}$) (Fig. S13b in ESI). Both peaks are well described by a single component, ruling out the coexistence of separate Au(0) and Au(I) species.[23] The measured $4f_{7/2}$ binding energy of **GBP2** lies between the typical values for bulk Au(0) (84.0 eV) and $Au_2(\mu$-DCPM)Cl_2, with a downshift of 0.46 eV relative to the precursor. This intermediate value, together with the uniform peak shape, indicates that all gold atoms in the polymer adopt a similar electronic environment carrying a partial positive charge ($Au^{+\delta}$), rather than a formal +1 state.[24] The negative shift from precursor to polymer reflects an increase in the electron density on Au upon chain formation, which supports the electron delocalization along the one-dimensional Au–Au backbone.

Given the unique electronic structure of **GBP2**, its intrinsic photoluminescence performance was further evaluated. It exhibits broad and complex luminescence in the solid state. The excitation spectra span a wide range from the UV to the visible region (Fig. S14 in ESI), indicating that the polymer could be efficiently excited at multiple excitation wavelengths (λ_{ex}s). Upon excitation at 360, 450, and 530 nm, the emission maxima were located at 490 (cyan), 530 (yellowish-green), and 595 nm (orange), respectively, showing a clear red-shift with increasing excitation wavelength (Fig. 3e and Fig. S15 in ESI). This λ_{ex}-dependent emission suggests a heterogeneous population of emissive species, which is consistent with the polydispersity of chain lengths in the one-dimensional GBP. The quantum yield of **GBP2** is 13.6% under excitation at 360 nm. Moreover, the delayed emission spectra are virtually identical to the prompt ones (Fig. S16 in ESI), and time-resolved measurements revealed millisecond-scale lifetimes at all the detection wavelengths (Fig. 3f). Similar prompt and delayed emission spectra were observed for **GBP1**, **GBP3**, and **GBP4** (Fig. S17 in ESI). These combined characteristics confirm the strong triplet nature of the excited states in these GBPs. Such highly efficient room-temperature phosphorescence is attributed to the heavy-atom effect of Au, which enhances spin-orbit coupling and promotes the intersystem crossing process.[25]

CONCLUSIONS

In summary, we systematically investigated the key factors governing the chain length of GBPs and achieved a record-high DP of 169 through the rational optimization of a one-pot synthesis strategy. The controlled release of Ag^+, electron-donating imidazole co-ligands, steric and electronic effects of the bisphosphine ligand, and reaction temperature are identified as crucial parameters for chain elongation. It is confirmed that the obtained polymer features a one-dimensional Au backbone with continuous Au—Au bonds and exhibits typical polymer characteristics. Spectroscopic investigations reveal pronounced electron delocalization along the Au backbone, leading to band-like electronic transitions and efficient phosphorescence. With gold as a demonstration, this work offers a viable strategy for constructing long-chain metal-backboned polymers and provides insights into the electronic properties of the one-dimensional metal backbones.

Conflict of Interests

Huisheng Peng is an editorial board member for *Chinese Journal of Polymer Science* and was not involved in the editorial review or the decision to publish this article. The authors declare no interest conflict.

Electronic Supplementary Information

Electronic supplementary information (ESI) is available free of charge in the online version of this article at http://doi.org/10.1007/s10118-026-3779-2.

Data Availability Statement

The data supporting the findings of this study are available from the corresponding authors upon reasonable request.

ACKNOWLEDGMENTS

This work was financially supported by the Ministry of Science and Technology of the People's Republic of China (Nos. 2022YFA1203001 and 2022YFA1203002), the National Natural Science Foundation of China (Nos. T2321003, T2596011, T2596012, and 22335003), and China Postdoctoral Science Foundation (No. 2025M780910). The authors would like to thank Prof. Kaiwen Zeng for his assistance with data analysis and discussion.

REFERENCES

1 Zeng, K.; Yang, Y.; Xu, J.; Wang, N.; Tang, W.; Xu, J.; Zhang, Y.; Wu, Y.; Xu, Y.; Wang, G.; Chen, P.; Wang, B.; Sun, X.; Jin, G.; Peng, H. Metal-backboned polymers with well-defined lengths. *Angew. Chem. Int. Ed.* **2023**, *62*, e202216060.
2 Zeng, K.; Peng, H. Metal-backboned polymer: conception,design and synthesis. *Chinese J. Polym. Sci.* **2023**, *41*, 3–6.
3 Zhang, Y.; Zeng, K.; Wu, Y.; Huang, F.; Peng, H. Synthesis of nickel-backboned polymers by incorporating triazine groups. *Sci. Bull.* **2025**, *70*, 2223–2227.
4 Wang, Z.; Chen, K.; Shi, X.; Du, Q.; Ai, Y.; Li, P.; Yong, L.; Sun, X.; Wang, N.; Hu, X.; Lu, C.; Tang, C.; Wang, L.; Zheng, Y.; Zhang, Y.;

Graphical Abstract

Chemically Bonding Metal Atoms into a Polymer Chain

Zihao Zhao, Fuyao Huang, Yifeng Zhang, and Huisheng Peng

Fudan University

Metal-backboned polymers with a polymerization degree of up to 169 were achieved by optimizing one-pot synthesis. They exhibit typical polymer behavior, pronounced electron delocalization along the backbone, and efficient room-temperature phosphorescence.

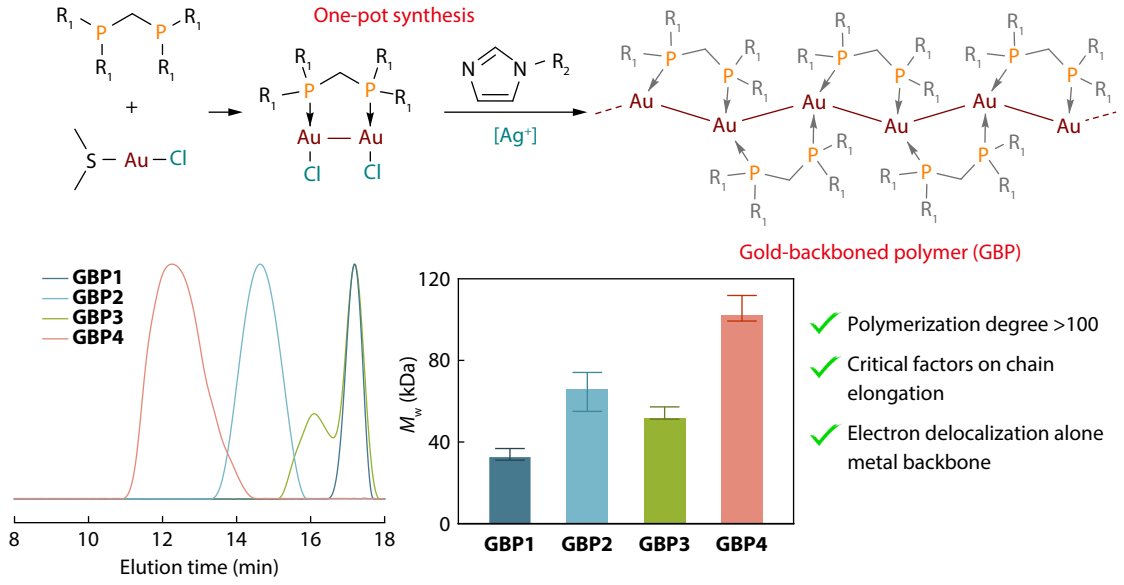

Chinese J. Polym. Sci., 2026 *https://doi.org/10.1007/s10118-026-3779-2*

Guo, H.; Pu, Z.; Wang, X.; Zhang, Y.; Jiang, H.; Liu, Y.; Tang, Z.; You, L.; Deng, J.; Che, R.; Gao, Y.; Zhang, S.; Wang, B.; Sun, X.; Qin, J.; Huang, Y.; Shen, L.; Ge, J.; Zeng, X.; Chen, L.; Chen, P.; Peng, H. Fibre integrated circuits by a multilayered spiral architecture. *Nature* **2026**, *650*, 102–109.

5 Zhang, Y.; Hao, S.; Wu, Y.; Huang, F.; Pang, J.; Wang, X.; Xu, X.; Zeng, K.; Zheng, G.; Peng, H. Cobalt-backboned oligomer for record photocatalytic CO_2 conversion to ethanol. *Angew. Chem. Int. Ed.* **2026**, *65*, e21378.

6 Wang, N.; Zeng, K.; Zheng, Y.; Jiang, H.; Yang, Y.; Zhang, Y.; Li, D.; Yu, S.; Ye, Q.; Peng, H. High-performance thermoelectric fibers from metal-backboned polymers for body-temperature wearable power devices. *Angew. Chem. Int. Ed* **2024**, *63*, e202403415.

7 Xu, J.; Zeng, K.; Zhang, Y.; Yang, Y.; Liu, Z.; Liu, Y.; Wang, J.; Zhang, K.; Wu, Y.; Sun, H.; Peng, H. High performance microwave absorption material based on metal-backboned polymer. *Chinese J. Polym. Sci*. **2024**, *42*, 1881–1887.

8 Vahrenkamp, H. What do we know about the metal-metal bond *Angew. Chem. Int. Ed*. **1978**, *17*, 379–392.

9 Mermin, N. D.; Wagner, H. Absence of ferromagnetism or antiferromagnetism in one- or two-dimensional isotropic heisenberg models. *Phys. Rev. Lett.* **1966**, *17*, 1133–1136.

10 Baletto, F.; Ferrando, R. Structural properties of nanoclusters: Energetic, thermodynamic, and kinetic effects. *Rev. Mod. Phys.* **2005**, *77*, 371–423.

11 Zhao, Z.; Huang, F.; Zhang, Y.; Hong, K.; Jiang, C.; Peng, H. One-pot synthesis of a long-chain metal-backboned polymer. *Natl. Sci. Rev*. **2026**, doi: 10.1093/nsr/nwag451.

12 Brandys, M.-C.; Jennings, M. C.; Puddephatt, R. J. Luminescent gold(I) macrocycles with diphosphine and 4,4'-bipyridyl ligands. *J. Chem. Soc. Dalton Trans*. **2000**, *29*, 4601–4606.

13 Yoshigoe, Y.; Tanji, Y.; Hata, Y.; Osakada, K.; Saito, S.; Kayahara, E.; Yamago, S.; Tsuchido, Y.; Kawai, H. Dynamic Au–C σ-bonds leading to an efficient synthesis of [n]cycloparaphenylenes (n = 9 – 15) by self-assembly. *JACS Au* **2022**, *2*, 1857–1868.

14 Angermair, K.; Bowmaker, G. A.; de Silva, E. N.; Healy, P. C.; Jones, B. E.; Schmidbaur, H. Vibrational and solid-state phosphorus-31 nuclear magnetic resonance spectroscopic studies of 1:1 complexes of PPh_3 with gold(I) halides; crystal structure of [AuBr(PMe_3)]. *J. Chem. Soc. Dalton Trans*. **1996**, *25*, 3121–3129.

15 Robin, J. H. C.; Joanne, H. T. A vibrational study by Raman speciroscopy of some dinuclear gold ylide complexes. *J. Organomet. Chem.* **1986**, *303*, 437–442.

16 O'Connor, A. E.; Mirzadeh, N.; Bhargava, S. K.; Easun, T. L.; Schröder, M.; Blake, A. J. Aurophilicity under pressure: a combined crystallographic and in situ spectroscopic study. *Chem. Commun.* **2016**, *52*, 6769–6772.

17 Schmidbaur, H.; Wohlleben, A.; Wagner, F.; Orama, O.; Huttner, G.

Gold-komplexe von diphosphinomethanen, I. synthese und kristallstruktur zweikerniger gold(I)-verbindungen. *Chem. Ber.* **1977**, *110*, 1748−1754.
18 Teets, T. S.; Nocera, D. G. Halogen photoreductive elimination from gold(III) centers. *J. Am. Chem. Soc.* **2009**, *131*, 7411−7420.
19 Schmidbaur, H.; Schier, A. A briefing on aurophilicity. *Chem. Soc. Rev.* **2008**, *37*, 1931−1951.
20 Yu, X.; Li, D.; Wang, K.; Xia, T.; Xu, C.; Wu, Z.; Cheng, L. The covalent AuI–AuI bond in (AuF)n (n = 2~4): A perspective to understand the closed-shell AuI···AuI interaction. *Inorg. Chem.* **2022**, *61*, 1051−1058.
21 Fu, W.-F.; Chan, K.-C.; Miskowski, V. M.; Che, C.-M. The Intrinsic 3[dσ*pσ] emission of binuclear gold(I) complexes with two bridging diphosphane ligands lies in the near UV; emissions in the visible region are due to exciplexes. *Angew. Chem. Int. Ed.* **1999**, *38*, 2783−2785.
22 Zhu, C.; Liang, J.; Wei, G. Theoretical investigation of an ultrastable one dimensional infinite monatomic mixed valent gold wire with excellent electronic properties. *Phys. Chem. Chem. Phys.* **2016**, *18*, 12338−12343.
23 Boccia, A.; Zanoni, R.; Arduini, A.; Pescatori, L.; Secchi, A. Negatively charged gold atoms in subnanometric particles: Experimental evidence from an X-ray photoelectron spectroscopy study. *J. Nanosci. Nanotechnol.* **2012**, *12*, 8851−8855.
24 Yamada, T.; Sekine, R.; Sawaguchi, T. Ultrahigh-vacuum multitechnique study of AuCN monolayers on Au(111) formed by electrochemical deposition. *J. Chem. Phys.* **2000**, *113*, 1217−1227.
25 Seifert, T. P.; Naina, V. R.; Feuerstein, T. J.; Knöfel, N. D.; Roesky, P. W. Molecular gold strings: aurophilicity, luminescence and structure–property correlations. *Nanoscale* **2020**, *12*, 20065−20088.

https://doi.org/10.1007/s10118-026-3779-2